Available online at www.sciencedirect.com
ScienceDirect
Polymer 48 (2007) 4449–4458
polymer
www.elsevier.com/locate/polymer

Study on the preparation and characterization of biodegradable polylactide/multi-walled carbon nanotubes nanocomposites

Chin-San Wu*, Hsin-Tzu Liao

Department of Biochemical Engineering and Graduate Institute of Environmental Polymer Materials, Kao Yuan University, Kaohsiung County 82101, Taiwan, ROC

Received 23 October 2006; received in revised form 2 June 2007; accepted 6 June 2007
Available online 9 June 2007

Abstract

In this study, polylactide/multi-walled carbon nanotubes (PLA/MWNTs) hybrids were prepared by means of a melt blending method. To enhance the compatibility between PLA and MWNTs, the acrylic acid grafted polylactide (PLA-*g*-AA) and the multihydroxyl-functionalized MWNTs (MWNTs−OH) were used to replace PLA and MWNTs, respectively. The crude MWNTs were chemically oxidized by a mixture of H_2SO_4 and HNO_3 and then reacted with thionyl chloride to functionalize them with chlorocarbonyl groups (MWNTs−COCl). The MWNTs−OH was finally obtained by the reaction of MWNTs−COCl and 1,6-hexanediol. The resulting products have been characterized by FTIR, ^{13}C solid-state NMR, TGA, DMA, SEM, TEM, and Instron mechanical tester. Due to the formation of ester groups through the reaction between carboxylic acid groups of PLA-*g*-AA and hydroxyl groups of MWNTs−OH, results demonstrated dramatic enhancement in thermal and mechanical properties of PLA, for example, 77 °C increase in initial decomposition temperature with the addition of only 1 wt%. Based on the result of thermal and mechanical examinations, it was found that the optimal amount of MWNTs−OH was 1 wt% because excess MWNTs−OH caused separation of the organic and inorganic phases and lowered their compatibility.

Keywords: Polylactide; Multi-walled carbon nanotubes; Melt blending

1. Introduction

The organic−inorganic nanocomposites have recently gained considerable interests in both the academic and industrial fields due to their unique mechanical, thermal, and electronic properties. In the past decades, the inorganic clay minerals, such as montmorillonite and hectrite, have been widely used as reinforcement materials for polymers due to their nanoscale size and intercalation/exfoliation properties [1−3]. At this scale, the inorganic fillers can improve dramatically the physical and mechanical macroscopic properties of polymer even though their amount is small. It is well known that carbon nanotubes (CNTs) have great potential for industrial application because they possess unique structure and properties [4]. Recently, a number of research groups have focused on the functionalization of CNTs, and then the modified CNTs are used to replace clay to prepare the polymer/CNTs nanocomposites [5−9].

However, to obtain the uniform dispersion of carbon nanotubes in the polymer matrix is very difficult due to the insolubility of the carbon nanotubes and the inherently poor compatibility between the carbon nanotubes and the polymer, and the resulting inhomogeneous nanocomposites often have unsatisfying properties. For the direct blending of CNTs and polymers, carbon nanotubes tend to aggregate, and their nonuniform dispersion in the polymer matrix often results in deleterious effects. Consequently, some methods must be proposed for functionalizing the carbon nanotubes (i.e., anchoring the matrix polymer on the carbon nanotubes) before using them as the fillers in the polymer matrix. Among those

* Corresponding author.
E-mail address: cws1222@cc.kyu.edu.tw (C.-S. Wu).

0032-3861/$ - see front matter © 2007 Elsevier Ltd. All rights reserved.
doi:10.1016/j.polymer.2007.06.004

methods, oxidatively generating carboxylic acid groups on the surface of the carbon nanotubes and then covalently linking oligomers or polymers with these carboxylic acid groups is an effective skill to improve the compatibility of hybrids [10–18]. Zeng et al. successfully anchored poly(ε-caprolactone) on the carbon nanotubes via the formation of ester linkages [16]. To date, two methodologies, namely noncovalent and covalent, have been developed to functionalize CNTs with a variety of organic, inorganic, metallic, biochemical, and polymeric structures [19,20]. Generally, the linkage of small or large molecules to the CNTs by covalent methods is more stable and effective than the noncovalent ones. So, the covalent methods, by which carboxylic acid groups formed at the ends and at the defect sites of CNTs, are commonly used for the precursor functionalization in the formation of ester and organometallic structures [21,22].

The use of non-renewable petroleum-based chemicals for the synthesis and manufacture of commercial polymers had caused many environmental problems associated with their disposal. The main strategies to address these problems are utilization of polymeric materials from renewable sources such as starch, cellulose and wood flour, and development of biodegradable polymeric materials such as polylactide (PLA), poly(ε-caprolactone) (PCL) and poly(3-hydroxybutyrate) (PHB). Polylactide (PLA), which can be produced by ring-opening polymerization of lactides and the lactic acid monomers used are obtained from the fermentation of sugar feed stocks, is a degradable thermoplastic polymer with excellent mechanical properties [23–26]. PLA has been found to degrade within a few weeks in soil environments [27]. However, PLA is not widely used because of its high cost as compared to synthetic plastics. To reduce cost, some articles have been proposed to study the composites of PLA and starch, and the result shows that the blends have rather poor mechanical properties due to poor adhesion of starch and PLA [28–30]. Varying types of chemicals, such as citrate esters, have been tried to plasticize PLA [31]. Recently, plasticizers such as poly(ethylene glycol) (PEG), glucose monoesters and partial fatty acid esters were used to improve the flexibility and impact resistance of PLA [32].

Nevertheless, the addition of carbon nanotubes as reinforced fillers to PLA has been less quantitatively understood in comparison with pure PLA, especially with respect to the effect of carbon nanotubes on the thermal and mechanical behaviors. The purpose of this study is devoted to prepare the nanocomposite from PLA and multi-walled carbon nanotubes (MWNTs) by a melt blending method. In this article, we report a new method for covalently linking the acrylic acid grafted polylactide (PLA-*g*-AA) to MWNTs. MWNTs were first chemically oxidized with strong oxidizing agents such as a mixture of HNO_3 and H_2SO_4, the generated carboxyls were next converted into hydroxyl groups by a treatment with thionyl chlorides and 1,6-hexanediol. Afterward, the hydroxyl group-functionalized MWNTs were used to blend with the PLA-*g*-AA to form nanocomposites. The sample was then thoroughly characterized with Fourier transform infrared (FTIR) spectroscopy, scanning electron microscopy (SEM), transmission electron microscopy (TEM), ^{13}C solid-state NMR, Instron mechanical tester, and thermal analysis techniques.

2. Experimental methods

2.1. Materials

The multi-walled carbon nanotubes (MWNTs, purity > 95%, diameter = 40–60 nm), produced via chemical vapor deposition (CVD), were purchased from Seasunnano Pro. Co. (China). Sulfuric acid (96%), nitric acid (61%), thionyl chloride, and 1,6-hexanediol were purchased from Aldrich Chemical Co. (Milwaukee, WI). Polylactide (PLA), composed of 95% L-lactide and 5% *meso*-lactide, was obtained from Nature Works Chemical Co. (Blair, Nebraska, USA). Acrylic acid (AA, Aldrich Chemical Co., Milwaukee, WI) was purified before use by re-crystallization from chloroform. The initiator, dicumyl peroxide (DCP, Aldrich Chemical Co., Milwaukee, WI), was recrystallized twice by dissolving it in absolute methanol. Other reagents were purified using the conventional methods. According to the procedures described in our previous work [33], the PLA-*g*-AA copolymer was made in our laboratory and its grafting percentage was about 5.96 wt%.

2.2. PLA-g-AA/MWNTs–OH hybrids' preparation

Scheme 1 illustrates our synthesis route to enhance the reactivity of MWNTs. The MWNTs were first chemically oxidized with a strong oxidizing agent (3/1 concentrated H_2SO_4/HNO_3 mixture) at 130–135 °C for 24 h to generate carboxyls onto them. The acid-treated samples (MWNTs–COOH) were stirred in $SOCl_2$ at 65–70 °C for 24 h under reflux to convert the carboxyls into acyl chlorides, and then the acyl chloride-functionalized MWNTs reacted with 1,6-hexanediol at 115–120 °C for 48 h, and this produced the hydroxyl group-functionalized MWNTs (MWNTs–OH). It can be found that the conversion of carboxylic acids into acid chlorides by the action of thionyl chlorides accompanied the formation of two very stable gaseous species (SO_2 and HCl). During the period of reaction, the SO_2 was continuously removed from the reaction as a gas to lower the extent of the reverse reaction. After the reaction was completed, the unreacted $SOCl_2$ was evaporated with a rotary evaporator and the collected MWNTs–COCl samples were dried in vacuum overnight. The –COCl group could be hydrolyzed readily into carboxylate ions in air due to its high reactivity. Consequently, the MWNTs–COCl samples should be kept away from air. The MWNTs–COCl was mixed with 1,6-hexanediol, the resulting solid was separated by vacuum-filtration using the 0.22 μm Millipore polycarbonate membrane filter and subsequently washed with anhydrous xylene. After repeated washing and filtration, the resulting solid (MWNTs–OH) was dried overnight in a vacuum oven. All the blends were prepared using a Brabender "Plastograph" 200Nm W50EHT mixer with a blade-type rotor. The rotor speed was set at 50 rpm and the blending reaction was carried out at

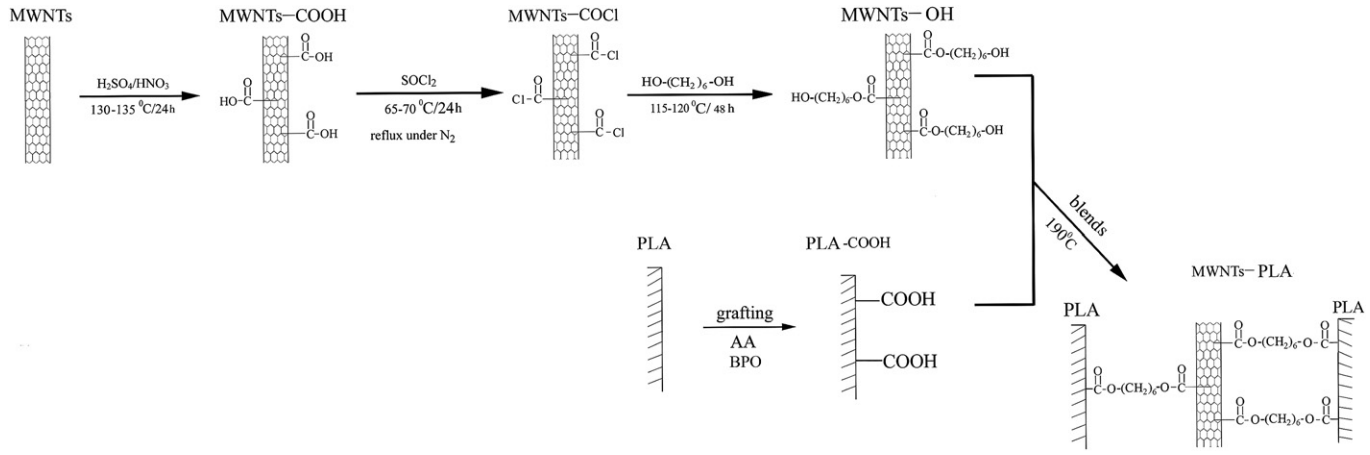

Scheme 1.

190 °C for 15 min. Prior to blending, the MWNTs–OH was dried in a vacuum oven at 60 °C for 2 days. The mass ratios of MWNTs–OH to PLA-*g*-AA were set at 0.5/99.5, 1/99, 2/98 and 3/97. After blending, the composite was pressed into 1-mm thick plate using a hydrolytic press at 190 °C and then put into a dryer for cooling. The cooled plates were made into standard specimens for further characterization. The relative humidity of the desiccator was set at 50 ± 5% and the samples were conditioned for 24 h. We found that 24 h of conditioning was adequate for dehydrating samples to appropriate water content and that a longer storage time did not have an appreciable effect on composite properties.

2.3. Characterizations of hybrids

The Fourier transform infrared spectrometry (BIO-RAD FTS-7PC type) was used to investigate the grafting reaction of acrylic acid onto PLA and to verify the incorporation of a MWNTs–OH phase to the extent that ester bonds were formed in hybrids. For the FTIR tests, the sample was ground into fine powders by the milling machine and then it was coated on a KBr plate. The ^{13}C solid-state NMR analysis was performed using a Bruker AMX 400 ^{13}C NMR spectrometer at the condition of 50 MHz. The NMR spectra were performed under cross-polarization; magic anodic angle sample spinning and power decoupling conditions with 90° pulse and 4 s cycle time. The glass transition temperature (T_g) and the melting temperature (T_m) of samples were determined from a TA Instrument 2010 DSC system (New Castle, DE). For DSC tests, sample sizes ranged from 4 to 6 mg and the T_g and T_m values were obtained from the melting curves recorded from −30 °C to 250 °C, scanned at a heating rate of 10 °C/min. To evaluate the compatibility of blends, the dynamic mechanical properties of blends were accomplished in a TA analyzer Model 2080 (New Castle, DE). The tests were performed at a frequency of 1 Hz, a strain level of 0.075%, and at a temperature range from −30 to 200 °C with a heating rate of 3 °C/min. The result of experiments performed in the linear region of elasticity and without causing drawing effects is chosen as the static force. To specify this force, several stress–strain experiments were performed beforehand and the ratio of static force to dynamic force was kept constant during the experiments. The thermogravimetry analyzer (TA Instrument 2010 TGA, New Castle, DE) was used to assess whether organic–inorganic phase interactions influenced thermal degradation of hybrids. Samples were placed in alumina crucibles and tested with a thermal ramp over the temperature range of 30–600 °C at a heating rate of 20 °C/min and then the initial decomposition temperatures (IDT) of hybrids were obtained. An XL-40FEG scanning electron microscope (SEM; Philips, Netherlands) was to study the morphology of the hybrids. Before testing, hybrids were prepared as thin films with a hydrolytic press, and films were then treated with hot water at 80 °C for 24 h. Afterward, the films were coated with gold and observed by SEM. A micrograph of a microtome section of the hybrids of 60–100 nm thickness, mounted in epoxy resin, was obtained with a transmission electron microscope (JEM-100CX II, Jeol Company, Japan) at an acceleration voltage of 100 kV. According to the ASTM D638 method, the Instron mechanical tester (Model LLOYD, LR5K type) was used to measure the tensile strength and strain at break. The films of testing samples, which were conditioned at 50 ± 5% relative humidity for 24 h prior to the measurements, were prepared in a hydrolytic press at 190 °C and then the measurements were carried out using a 20 mm/min crosshead speed. Five measurements were performed for each sample and the results were averaged to obtain a mean value.

3. Results and discussion

3.1. FTIR/NMR analysis

The FTIR spectrum of MWNTs–COOH, which was obtained from the chemical oxidation of MWNTs by the strong oxidizing acid [(96%) H_2SO_4/(65%) HNO_3 = 1/3], was thoroughly studied in this work and the result is illustrated in Fig. 1B. Similar to the findings of Huang et al. [34], all the

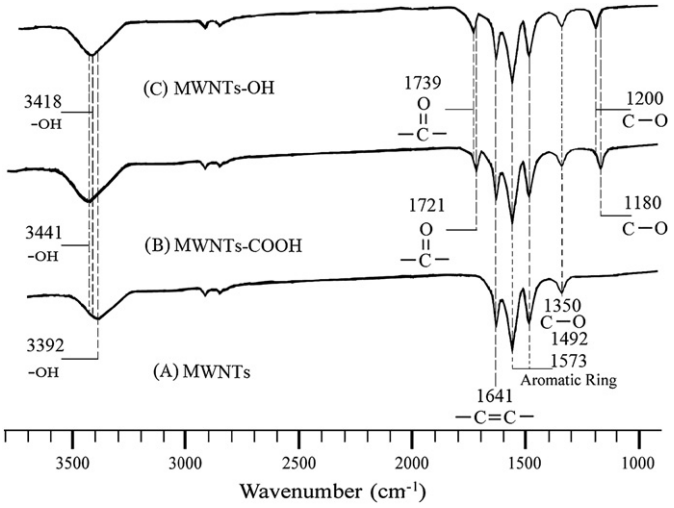

Fig. 1. FTIR spectra of (A) MWNTs, (B) MWNTs−COOH, and (B) MWNTs−OH.

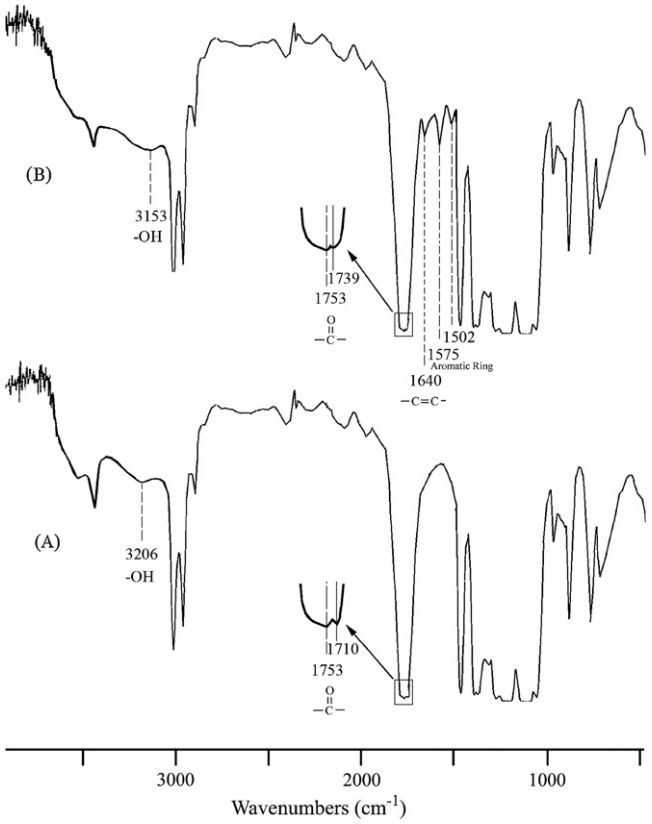

Fig. 2. FTIR spectra for (A) PLA-*g*-AA and (B) PLA-*g*-AA/MWNTs−OH (1 wt%).

characteristic peaks of MWNTs−COOH appeared at 1180 and 1350 cm^{-1} (C−O), 1600−1450 cm^{-1} (aromatic ring), 1641 cm^{-1} (C═C), 1721 cm^{-1} (C═O), and 3441 cm^{-1} (−OH). As compared with the FTIR spectrum of MWNTs (Fig. 1A), the peaks appearing at around 1721 and 1180 cm^{-1} in Fig. 1B were from the stretching vibration of C═O and −C−O groups in the carboxyl group (−COOH), respectively. This result showed that the long ropes of MWNTs were cleaved into short open-ended pipes and that both the tube ends and the sidewalls were covered with the oxygen-containing functional groups, such as carboxyls (−COOH), carbonyls (−C═O), and hydroxyls (−OH) after treatment of chemical oxidation [35,36]. These attached functional groups therefore corroborated the successful carboxylate ions of MWNTs and then enhanced the reactivity of MWNTs. The −COOH of MWNTs−COOH was transformed into acyl chloride functionalities by the action of thionyl chlorides ($SOCl_2$) and the distinctive stretching vibration of −COCl should have been observed. However, the detection of the stretching vibration of −COCl in the FTIR spectrum (operated in air) is extremely difficult because the high hydrolytic reactivity of −COCl in air tended to convert them back into carboxylate ions. To form the stronger chemical bonds (−OH), the MWNTs−COCl reacted with 1,6-hexanediol to produce the MWNTs−OH and the result of FTIR analysis is shown in Fig. 1C. From the result shown in Fig. 1C, it was found that the peaks arose from the stretching vibration of C═O and −C−O groups in the ester group are shifted from 1721 and 1180 to 1739 and 1200 cm^{-1}, respectively [19,37]. This observation confirmed that −COCl group of MWNTs−COCl can react with 1,6-hexanediol to form MWNTs−OH. Comparing the FTIR spectra of MWNTs−COOH and MWNTs−OH, it was also found that the hydroxyl-stretching band appeared as a strong broad band at 3441 cm^{-1} for the MWNTs−COOH but it shifted to 3418 cm^{-1} for the MWNTs−OH. This further band at 3418 cm^{-1} was assigned to octahedral vacancies and designated as MWNTs−OH. This region at 3200−3500 cm^{-1} was therefore identified as being representative of non-hydrogen bonded hydroxyl groups (labeled as isolated or free hydroxyl groups).

The FTIR spectrum of the AA grafted PLA (PLA-*g*-AA) is shown in Fig. 2A. It can be seen that, besides an extra peak at 1710 cm^{-1}, assigned to −C═O, as well as a broad O−H stretching absorbance at 3200−3700 cm^{-1}, all the characteristic peaks of PLA at 3300−3700, 1700−1760 and 500−1500 cm^{-1} appeared in the PLA-*g*-AA [33]. This pattern of peaks demonstrated that acrylic acid had been grafted onto the PLA matrix because the discernible shoulder near 1710 cm^{-1} revealed the formation of free acid in the modified polymer. Furthermore, Fig. 2B illustrates the FTIR spectrum of the MWNT−CO−O−$(CH_2)_6$−O−OC−PLA blend, and the result showed that strong absorption for aromatics in the region of 1600−1450 cm^{-1} occurred as a result of the condensation reaction between MWNTs−OH and PLA-*g*-AA [38]. It was also found that the peak at 1710 cm^{-1} shown in Fig. 2A was shifted to 1739 cm^{-1} due to the formation of ester groups through the reaction between carboxylic acid groups of PLA-*g*-AA and hydroxyl groups of MWNTs−OH [39]. For the PLA-*g*-AA copolymer (Fig. 2A), the hydroxyl-stretching band appears as a strong broad band at 3206 cm^{-1}. For PLA-*g*-AA/MWNTs−OH hybrids (Fig. 2B), the vibration bands broadened with increased MWNTs−OH content and shifted to 3153 cm^{-1} for 1 wt% MWNTs−OH. The reason for the shift in wave number is the presence of H_2O formed from esterification of −COOH and MWNTs−OH.

To further confirm the grafting of AA onto PLA and to investigate compatibility between PLA-*g*-AA and MWNTs–OH, ^{13}C NMR was used to examine the structure of PLA-*g*-AA and PLA-*g*-AA/MWNTs–OH and the result is shown in Fig. 3. For the pure PLA, as the result of our previous work [33] and Breitenbach et al. [40], carbon peaks occurred in three places (1: $\delta = 16.91$ ppm, 2: $\delta = 68.75$ ppm, and 3: $\delta = 169.36$ ppm). The ^{13}C NMR spectrum of PLA-*g*-AA (Fig. 3A) showed that there were three extra peaks (C_β: $\delta = 35.59$ ppm; C_α: $\delta = 42.23$ ppm; a: $\delta = 174.96$ ppm). These extra peaks (C_α, C_β and "a") confirmed that AA had been indeed grafted onto PLA, and the corresponding structure is illustrated in Fig. 3A [33]. Comparing the ^{13}C solid-state NMR spectra of PLA-*g*-AA and PLA-*g*-AA/MWNTs–OH, the latter revealed extra peaks at $\delta = 120$–125 ppm (aromatic carbon of MWNTs) and the peak at $\delta = 174.96$ ppm (C=O) was absent in PLA-*g*-AA/MWNTs–OH but shifted this peak to the duplicates at $\delta = 178.06$ ppm due to the reaction between –COOH of PLA-*g*-AA and –OH of MWNTs–OH. This provides further evidence of the condensation between PLA-*g*-AA and MWNTs–OH, and confers the conclusion that the original MWNTs–OH was fully hydroxyl, and that in this reaction the hydroxyl groups were converted into ester (represented by peaks $\delta = 178.06$ ppm). Formation of ester functional groups has a profound effect on thermal and mechanical properties, something that will be discussed in the following sections.

3.2. DMA analysis

The dynamic mechanical properties of PLA-*g*-AA and PLA-*g*-AA/MWNTs–OH were measured and used to evaluate the compatibility of hybrids. Fig. 4 shows variations of the loss tangent (tan δ) with temperature for the PLA-*g*-AA and PLA-*g*-AA/MWNTs–OH hybrids, and the result shows that the tan δ increases sharply at a particular temperature, while the onset of segmental motion starts. In the case of PLA-*g*-AA/MWNTs–OH hybrids, the peak generally broadens and decreases in intensity with an increasing MWNTs–OH content. Moreover, the damping temperature, at which a displaced maximum occurred due to the glass transition of PLA-*g*-AA, was increased markedly from 64.8 to 73.5 °C as the MWNTs–OH content was increased from 0 to 1 wt% because the inorganic network hinders segmental motions of the polymer chains. The shifts in tan δ to higher temperatures in the PLA-*g*-AA/MWNTs–OH hybrids suggested increased adhesion between the polymer and the MWNTs–OH in this system. It is also found that the increment on the damping temperature of hybrids becomes slight when the MWNTs–OH content is greater than 1 wt%. So, the most efficient bonding was seen in PLA-*g*-AA/MWNTs–OH with 1 wt% MWNTs–OH, the subsequent slow increase in damping temperature at which the peak occurred with MWNTs–OH contents above 1 wt% may be due to excess MWNTs–OH causing separation of the organic and inorganic phases and lowering their compatibility. It is concluded, therefore, that the good interfacial interactions occurred at approximately 1 wt% MWNTs–OH [5].

3.3. DSC/TGA analysis

The thermal properties of hybrids with various MWNTs–OH contents were obtained via DSC and TGA tests, and the

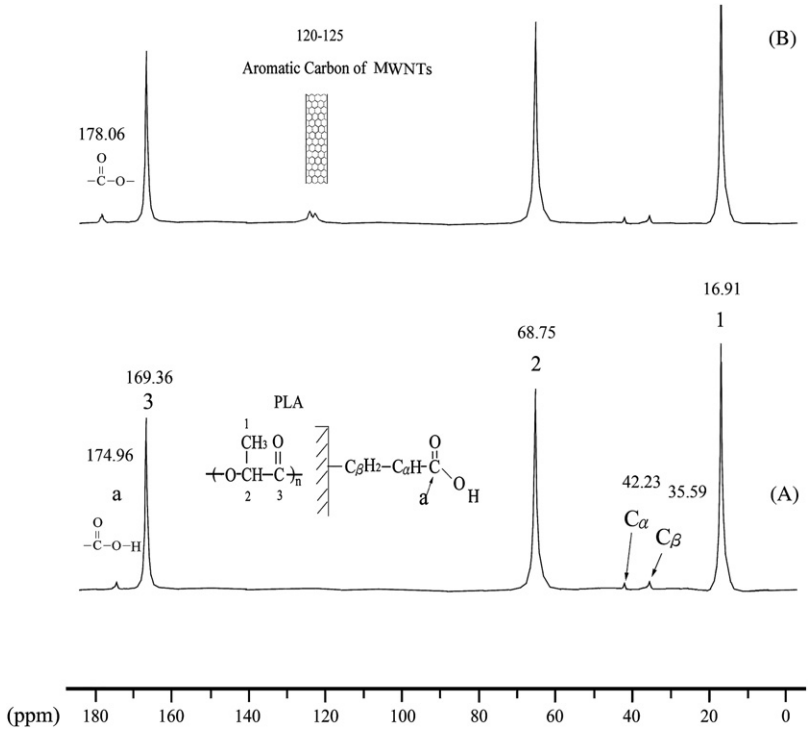

Fig. 3. ^{13}C solid-state NMR spectra of (A) PLA-*g*-AA and (B) PLA-*g*-AA/MWNTs–OH (1 wt%).

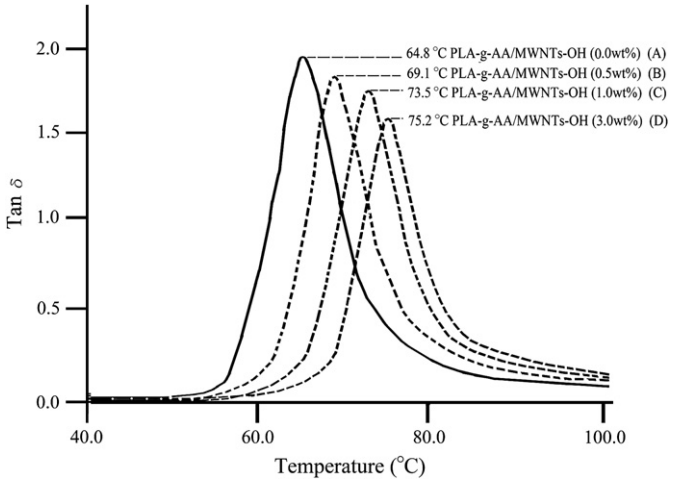

Fig. 4. Variation of the tan δ with temperature for PLA-*g*-AA and its blends with different contents of MWNTs−OH.

results are shown in Figs. 5 and 6. The glass transition temperature (T_g) of the hybrid composites is associated with a cooperative motion of long-chain segments, which may be hindered by the MWNTs−OH. Therefore, as expected, PLA-*g*-AA/MWNTs−OH recorded higher glass transition temperatures than the PLA-*g*-AA copolymer (Fig. 5). It may be suggested that the enhancement in T_g for PLA-*g*-AA/MWNTs−OH hybrids is due to the reason that the MWNTs−OH phase was able to form chemical bonds on hydroxyl group sites provided by the carboxylic acid groups of PLA-*g*-AA. These strong bonds are able to hinder the motion of the polymer chains. Similar to the result of DMA test, it can be seen that the enhancement in the T_g was not marked for the MWNTs−OH content beyond 1 wt%. This result might be due to the low grafting percentage (about 5.96 wt%) of the PLA-*g*-AA copolymer since the increment of T_g is dependent on the number of functional groups in the copolymer matrix to

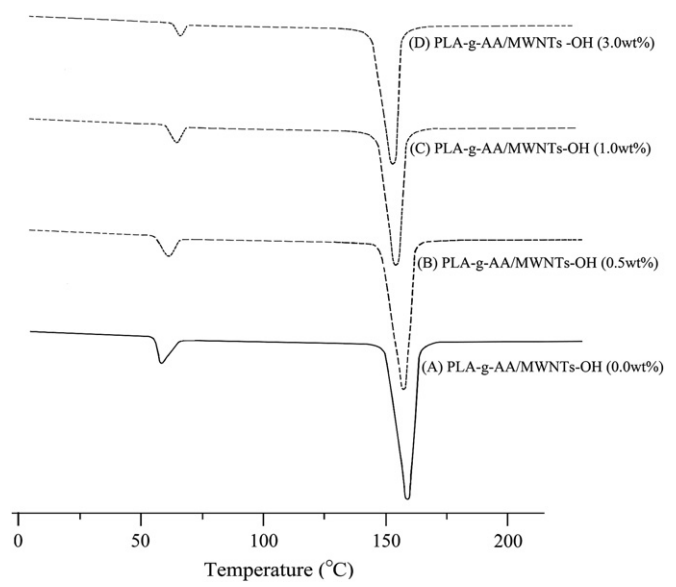

Fig. 5. DSC heating thermograms of PLA-*g*-AA and its blends with different contents of MWNTs−OH.

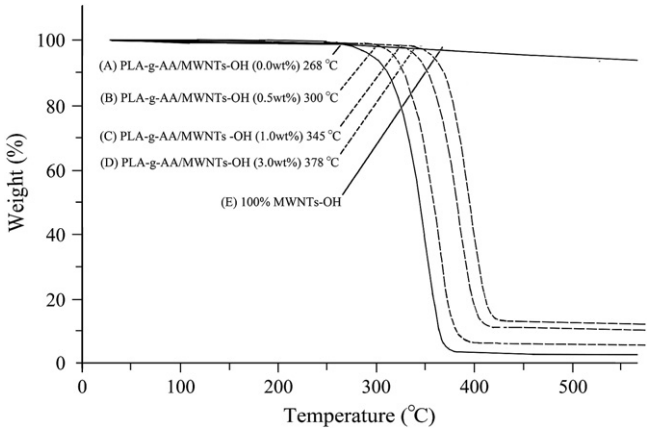

Fig. 6. TGA curves for PLA-*g*-AA and its blends with different contents of MWNTs−OH.

react with the hydroxyl groups in the MWNTs−OH [41]. With MWNTs−OH content above 1 wt%, they were dispersed physically in the polymer matrix. Such excess MWNTs−OH might have caused separation of the organic and inorganic phases and lowered their compatibility, causing the enhancement on the T_g value. Fig. 5 also shows that the melting temperature (T_m) decreased markedly with an increasing MWNTs−OH content up to 1 wt% and then the effect was slight. The marked decrease in T_m of PLA-*g*-AA/MWNTs−OH is probably the result of the MWNTs−OH prohibiting the movement of the polymer segments, causing polymer chain arrangement to become more difficult, and also of the hydrophilic character of MWNTs−OH leading to poor adhesion with the hydrophobic PLA. Tables 1 and 2 summarize the thermal and mechanical properties (T_g, T_m, ΔH_m, IDT, and TS) of PLA/MWNTs and PLA-*g*-AA/MWNTs−OH hybrids. As expected, both PLA/MWNTs and PLA-*g*-AA/MWNTs−OH recorded higher glass transition temperatures than pure PLA (Table 1). It was also found that the enhancement in T_g for PLA-*g*-AA/MWNTs−OH hybrids was more significant than that for PLA/MWNTs hybrids. This is because the MWNTs−OH phase was able to form chemical bonds on −COOH sites provided by the carboxylic acid groups of PLA-*g*-AA/MWNTs−OH. These bonds are stronger than the hydrogen bonds in PLA/MWNTs and therefore are able to hinder the motion of the polymer chains. Table 1 also shows how the melting temperature (T_m) decreased with increasing MWNTs or MWNTs−OH content for PLA/MWNTs, whereas

Table 1
Glass transition temperature and melt temperature of PLA/MWNTs and PLA-*g*-AA/MWNTs hybrids

MWNTs or MWNTs−OH (wt%)	PLA/MWNTs		PLA-*g*-AA/MWNTs−OH	
	T_g (°C)	T_m (°C)	T_g (°C)	T_m (°C)
0	57.8	160.5	56.9	158.7
0.5	58.5	159.3	61.6	156.3
1.0	59.6	158.2	64.1	153.2
2.0	60.5	157.3	65.2	152.6
3.0	61.3	156.5	65.9	152.0

Table 2
Thermal and mechanical properties of PLA/MWNTs and PLA-*g*-AA/MWNTs hybrids

MWNTs or MWNTs–OH (wt%)	PLA/MWNTs			PLA-*g*-AA/MWNTs–OH		
	IDT (°C)	ΔH_m (J/g)	TS (MPa)	IDT (°C)	ΔH_m (J/g)	TS (MPa)
0	273	38.2 ± 0.8	52.3 ± 0.7	268	36.8 ± 0.7	48.8 ± 0.8
0.5	280	33.6 ± 0.7	53.6 ± 1.1	300	35.6 ± 0.7	56.6 ± 1.3
1.0	301	29.8 ± 0.5	55.1 ± 1.2	345	33.8 ± 0.6	62.3 ± 1.5
2.0	318	25.5 ± 0.5	56.0 ± 1.3	361	31.3 ± 0.6	63.1 ± 1.6
3.0	335	23.7 ± 0.4	56.5 ± 1.2	378	28.6 ± 0.5	63.9 ± 1.7

for PLA-*g*-AA/MWNTs–OH, the lowest T_m occurred at 1 wt% MWNTs or MWNTs–OH. Notably, T_m values for all PLA-*g*-AA/MWNTs–OH hybrids were lower than their PLA/MWNTs equivalents. This lower melting temperature of PLA-*g*-AA/MWNTs–OH makes it a more easily processed blend.

Table 2 shows that the melt heat (ΔH_m) of pure PLA was 38.2 ± 0.8 J/g. The value of this parameter increased with the crystal formation while it decreased as the MWNTs or MWNTs–OH content increased. The decrease in crystallization was probably caused by increased difficulty in arranging the polymer chain because of MWNTs or MWNTs–OH prohibiting movement of the polymer segments. Another potential cause is the hydrophilic character of MWNTs or MWNTs–OH, which would lead to poor adhesion with the hydrophobic PLA. Table 2 also shows that ΔH_m decreased with increasing MWNTs or MWNTs–OH content for both PLA/MWNTs and PLA-*g*-AA/MWNTs–OH. Additionally, ΔH_m was about 2–6 J/g higher with PLA-*g*-AA in the composite in place of PLA. Higher ΔH_m is caused by the formation of the ester carbonyl functional group from the reaction between the –OH group of MWNTs–OH and the –COOH group of PLA-*g*-AA.

It is known that the defunctionalization of carbon nanotubes can be realized by thermal decomposition. In the present study, we used the thermal gravity analysis (TGA) to determine the effect of MWNTs–OH content on the weight loss of hybrids, and the result is illustrated in Fig. 6 and Table 2. The initially degraded temperatures of PLA-*g*-AA and hybrids with MWNTs–OH contents of 0.5, 1.0, and 3 wt% are 268, 300, 345, and 378 °C, respectively. It is also found that the MWNTs–OH is not degraded up to 500 °C. The increase in the initially degraded temperature (IDT) was probably caused by the increased difficulty in arranging the polymer chain, due to MWNTs–OH prohibiting the movement of the polymer segments. Another potential cause is the character of MWNTs–OH, which would lead to condensation reaction adhesion with the PLA-*g*-AA. Kashiwagi et al. [42] studied the properties of polypropylene/clay nanocomposites and reported similar phenomena. According to these TGA traces, the increment of IDT is about 80 °C for 1 wt% MWNTs–OH but the increment is only 33 °C as the MWNTs–OH content is increased from 1 to 3 wt%. This result further confirmed that the optimal loading of MWNTs–OH is 1 wt% because excess MWNTs–OH will cause separation of the organic and inorganic phases and lowering their compatibility. In addition, the residual yields of the PLA-*g*-AA/MWNTs–OH nanocomposites increased with increasing MWNTs–OH content, indicating that thermal decomposition of the polymer matrix was retarded in the PLA-*g*-AA/MWNTs–OH nanocomposites with higher residual yield. This result may be attributed to a physical barrier effect, resulting from the fact that MWNTs–OH would prevent the transport of decomposition products in the polymer nanocomposites. Similar observations have reported that the thermal stability of polypropylene/MWNTs nanocomposites was improved by a physical barrier effect, enhanced by ablative reassembling of the MWNTs layer [43]. Therefore, the TGA results demonstrate that the incorporation of a small quantity of MWNTs–OH can significantly improve the thermal stability of the PLA-*g*-AA/MWNTs–OH nanocomposites. Both the PLA/MWNTs and PLA-*g*-AA/MWNTs–OH hybrids raised the IDT value (Table 2). Moreover, despite PLA-*g*-AA having a lower IDT value than PLA, the PLA-*g*-AA/MWNTs–OH hybrids produced IDT values higher than those of the equivalent PLA/MWNTs. This outcome is a result of the difference in interfacial forces in the two hybrids: the weaker hydrogen bonds of PLA/MWNTs compared with the stronger coordination sites associated with the carboxylic acid groups of AA and the –OH group of MWNTs–OH. Table 2 also shows that the increment of IDT for both hybrids was not significant with MWNTs or MWNTs–OH content above 1 wt%. This was because the formation of agglomerates can be observed for higher filler content (Fig. 8).

3.4. Hybrid morphology

It is necessary to study the morphology of the MWNTs–OH and polymer blends since the mechanical properties depend on it. In general, the good dispersion of MWNTs–OH in the polymer matrix, effective functional groups of MWNTs–OH, and the strong interfacial adhesion between two phases are required to obtain a composite material with satisfactory mechanical properties. The scanning electron microscopy (SEM) was used to study the tensile fractured surfaces of PLA/MWNTs (1 wt%) and PLA-*g*-AA/MWNTs–OH (1 wt%) blends, and the SEM microphotographs are shown in Fig. 7. As shown in the SEM photo of pristine MWNTs–OH (Fig. 7A), many entangled clusters of MWNTs–OH are observed. In the blends studied in this work, the major component (PLA or PLA-*g*-AA) forms the matrix, whereas the minor component (MWNTs or MWNTs–OH) is the dispersed phase. It is clear that the individually embedded MWNTs–OH

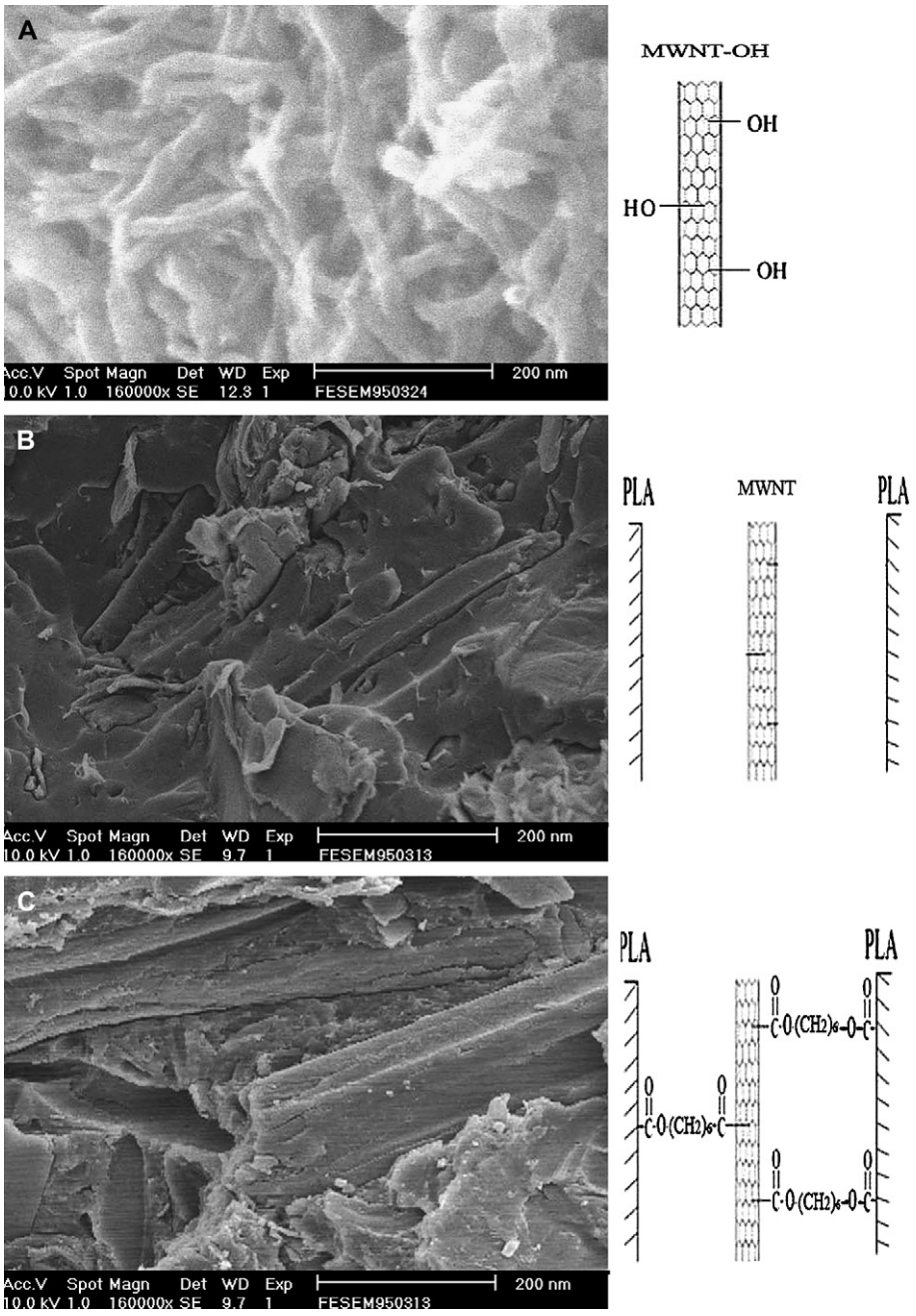

Fig. 7. SEM micrographs of (A) MWNTs−OH, (B) tensile fracture surfaces of PLA/MWNTs (1 wt%), and (C) tensile fracture surfaces of PLA-*g*-AA/MWNTs−OH (1 wt%).

in the polymer matrix is really difficult to find if insufficient dispersion and poor interfacial adhesion between filler and matrix occur. So, the lack of wettability may lead to some agglomerated MWNTs−OH clusters. Fig. 7B shows the poor wetting of MWNTs for PLA/MWNTs hybrid. The reason for this is the large difference in the surface energy between MWNTs and the PLA matrix. However, these entangled clusters were not found on the SEM microphotograph of the fractured surface of the PLA-*g*-AA/MWNTs−OH hybrid (Fig. 7C). It is also found that the MWNTs−OH is embedded in the PLA-*g*-AA matrix, and that smooth interfaces between MWNTs−OH and PLA-*g*-AA are observed, so that the MWNTs−OH is considered to have good wettability for PLA-*g*-AA. Further, the PLA-*g*-AA chains on MWNTs−OH might help the compatibility between MWNTs−OH and PLA-*g*-AA matrix. All these support the wettability of MWNTs−OH in PLA-*g*-AA. The reason for this result is that the properties of MWNTs−OH surfaces and PLA-*g*-AA matrix become more similar because the PLA-*g*-AA/MWNTs−OH blend can produce branched ester bonds from the condensation reaction between them. The fine nanostructures of the PLA-*g*-AA/MWNTs−OH hybrid were further investigated at high magnification as demonstrated in Fig. 8. As shown in Fig. 8, the MWNTs−OH can be dispersed

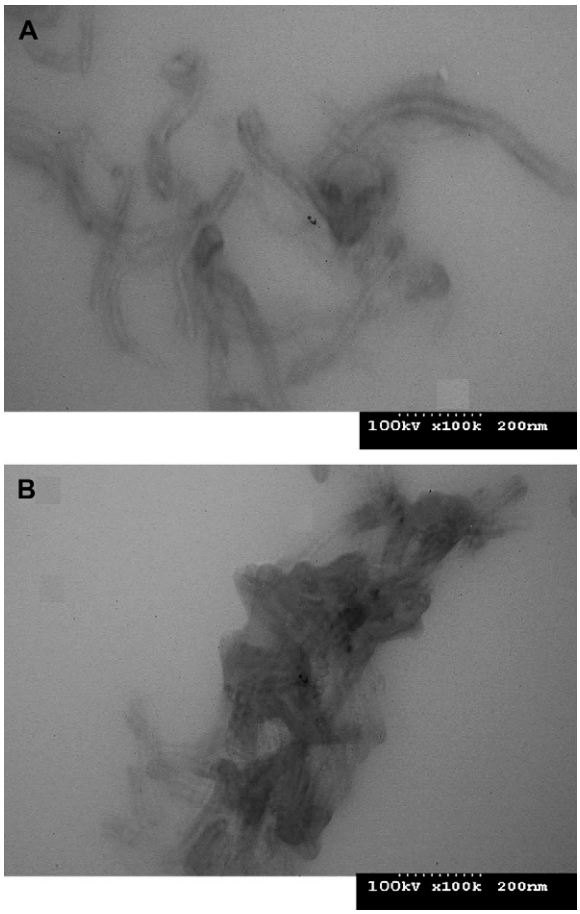

Fig. 8. TEM micrographs of (A) PLA-*g*-AA/MWNTs–OH (1 wt%) and (B) PLA-*g*-AA/MWNTs–OH (3 wt%).

well in the polymer matrix for 1 wt% of MWNTs–OH but the formation of agglomerates can be observed for 3 wt% MWNTs–OH.

3.5. Mechanical properties of hybrids

The stress–strain curves of the PLA-*g*-AA/MWNTs–OH nanocomposites with different MWNTs–OH content are shown in Fig. 9. In all cases the curves are linear at low strain followed by plastic deformation in the region of 2% strain. At higher strains the films yield up to a breaking strain of 4% for the PLA-*g*-AA. This breaking strain tends to decrease with increasing MWNTs–OH content and occurs at approximately 2.5% for the 3 wt% composite followed by a stiffening of the material [44]. Similar to the effect of MWNTs–OH content on the thermal property, it can be seen from Fig. 9 that the tensile strength of PLA-*g*-AA/MWNTs–OH hybrids increases rapidly with the increasing MWNTs–OH content from 0 to 1 wt% and then the tensile strength improves slightly. The positive effect on tensile strength may be due to the stiffness of the MWNTs–OH layers contributing to the presence of immobilized or partially immobilized polymer phases [45], high aspect ratio and surface area of the carbon nanotubes, and the nanoscale dispersion of MWNTs–OH

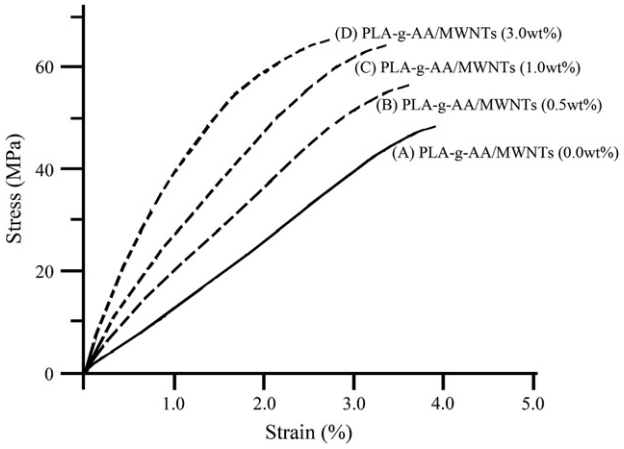

Fig. 9. Representative stress–strain curves for PLA-*g*-AA-based composites for a range of MWNTs–OH content.

layers in the polymer matrix. It is also possible that MWNTs–OH layer orientation as well as molecular orientation contribute to the observed reinforcement effect. The slight decrement in tensile strength for the MWNTs–OH content above 1 wt% could be attributed to the inevitable aggregation of the MWNTs–OH in high MWNTs–OH content. These results support the theoretical and molecular simulation predictions that stress transfer, and hence strength, of nanotube–polymer composites can be effectively increased by the formation of chemical bonding between them [5,46,47]. The variation of tensile strength with different filler content for PLA/MWNTs and PLA-*g*-AA/MWNTs–OH hybrids is illustrated in Table 2. For PLA/MWNTs hybrids, it is clear that the effect of MWNTs content on the tensile strength is somewhat insignificant because the interfacial force between the PLA matrix and the MWNTs is only one of the relatively weak hydrogen bonds. The PLA-*g*-AA/MWNTs–OH hybrid exhibited much better tensile strength than the equivalent PLA/MWNTs, even though PLA-*g*-AA had a lower tensile strength than pure PLA. The enhancement in tensile strength was attributed to the presence of the MWNTs–OH and the consequent formation of chemical bonds, through the dehydration of carboxylic acid groups in PLA-*g*-AA. However, the tensile strength of the PLA-*g*-AA/MWNTs–OH hybrid increased markedly with an increasing MWNTs–OH content up to 1 wt% and then approached a plateau. This, similar to the deterioration in other properties above 1 wt% MWNTs–OH, is due to the formation of agglomerates of MWNTs–OH.

4. Conclusions

We report the synthesis of PLA-*g*-AA/MWNTs–OH nanocomposites by using the simple melt blending method. For the modification of MWNTs, the process involves the chemical oxidation to cleave MWNTs and to open the tube ends, the creation of acyl chloride functionalities on the MWNTs, and the conversion of acyl chlorides into hydroxyls with excess 1,6-hexanediol. Hydroxyl groups' functionalization makes the carbon nanotubes a very effective side chain. We have

demonstrated that the MWNTs–OH can be incorporated into the PLA-*g*-AA copolymer through the formation of strong covalent bonds produced from the reaction between carboxylic acid groups of PLA-*g*-AA and hydroxyl groups of MWNTs–OH. Thus, MWNTs–OH can play a reinforcement role in the PLA-*g*-AA polymer matrix. FTIR and ^{13}C solid-state NMR spectra showed that the acrylic acid had been grafted onto the PLA copolymer and that ester bonds had formed in the PLA-*g*-AA/MWNTs–OH hybrid. The newly formed ester bonds may be produced through dehydration of carboxylic acid groups in the PLA-*g*-AA matrix with grafted hydroxyl groups in the MWNTs–OH. The SEM microphotographs give the result that the wettability of MWNTs–OH in PLA-*g*-AA is much better than the wettability of MWNTs in PLA. The TEM examination also proves that the formation of agglomerates of carbon nanotubes can be observed for hybrids with higher MWNTs–OH content. As the result of DSC analysis, it can be found that the gap between T_g and T_m of the PLA-*g*-AA/MWNTs–OH hybrid is smaller than that of the PLA/MWNTs hybrid. This implied that the compatibility between PLA and MWNTs has been enhanced. TGA tests showed that the PLA-*g*-AA/MWNTs–OH hybrid with 1 wt% MWNTs–OH gives an increment of 77 °C for the initial decomposition temperature. The effect of MWNTs–OH content on tensile strength at break of PLA-*g*-AA/MWNTs–OH hybrids was similar. Maximum values of tensile strength of hybrid occurred at about 1 wt% of MWNTs–OH and excess MWNTs–OH reduced the compatibility of hybrid due to the inevitable aggregation of carbon nanotubes.

References

[1] Tseng CR, Wu JY, Lee YH, Chang FC. Polymer 2001;42:10063.
[2] Vaia RA, Ishii H, Giannelis EP. Chem Mater 1993;5:1694.
[3] Okamoto M, Morita S, Kotaka T. Polymer 2001;42:2685.
[4] Ijima S. Nature 2001;13:3823.
[5] Yao Z, Braidy N, Botton GA, Adronov A. J Am Chem Soc 2003; 125:16015.
[6] Qin S, Qin D, Ford WT, Resasco DE, Herrera JE. Macromolecules 2004;37:752.
[7] Lepoitevin B, Pantoustier N, Alexandre M, Calberg C, Jerome R, Dubois P. J Mater Chem 2002;12:3528.
[8] Fisher FT, Bradshaw RD, Brinson LC. Appl Phys Lett 2002;80:4647.
[9] Chen J, Ramasubramaniam R, Xue C, Liu H. Adv Funct Mater 2006;16:114.
[10] Liu I-C, Huang HM, Chang CY, Tsai HC, Hsu CH, Tsiang RCC. Macromolecules 2004;37:283.
[11] Hu H, Ni Y, Montana V, Haddon RC, Parpura V. Nano Lett 2004;4:507.
[12] Lin J, Rinzler AG, Dai H, Hafner JH, Bradley RK, Boul PJ, et al. Science 1998;280:1253.
[13] Baskaran D, Mays JW, Bratcher MS. Nanotechnology 2004;37:4022.
[14] Zhang Y, Li J, Shen Y, Wang M, Li J. J Phys Chem B 2004; 108:15343.
[15] Chen J, Hamon MA, Hu H, Chen Y, Rao AM, Eklund PC, et al. Science 1998;282:95.
[16] Zeng H, Gao C, Yan D. Adv Funct Mater 2006;16:812.
[17] Zhang J, Zou H, Qing Q, Yang Y, Li Q, Liu Z, et al. J Phys Chem B 2003;107:3712.
[18] Jung YC, Sahoo NG, Cho JW. Macromol Rapid Commun 2006;27:126.
[19] Besteman K, Lee JO, Wiertz FGM, Heering HA, Dekker C. Nano Lett 2003;3:727.
[20] Lin Y, Zhou B, Fernando KAS, Liu P, Allard LF, Sun YP. Macromolecules 2003;36:7199.
[21] Zhu J, Peng H, Rodriguez-Macias Fernando, Margrave JL, Khabashesku VN, Imam AM, et al. Adv Funct Mater 2004;14:643.
[22] Sano M, Kamino A, Okamura J, Shinkai S. Langmuir 2001;17:5125.
[23] Tsuji H, Ikada Y. J Appl Polym Sci 1998;67:405.
[24] Lunt J. Polym Degrad Stab 1998;59:145–52.
[25] Drumright RE, Gruber PR, Henton DE. Adv Mater 2000;12:1841.
[26] Hakkarainen M. Adv Polym Sci 2002;157:113.
[27] Shogren RL, Doane WM, Garlotta D, Lawton JW, Willett JL. Polym Degrad Stab 2003;79:405.
[28] Kim SH, Chin I, Yoon J, Kim SH, Jung J. Korea Polym J 1998;6: 422.
[29] Ke T, Sun X. Cereal Chem 2000;77:761.
[30] Park YD, Tirelli N, Hubbell JA. Biomaterials 2003;24:893.
[31] Martin O, Averous L. Polymer 2001;42:6209.
[32] Hoffman AS. Adv Drug Delivery Rev 2002;43:3.
[33] Wu CS, Liao HT. Polymer 2005;46:10017.
[34] Huang HM, Lin IC, Chang CY, Tsai HC, Hsu CH, Tsiang RC. J Polym Sci Part A Polym Chem 2004;42:5802.
[35] Zhang J. J Phys Chem B 2003;107:3712.
[36] Kuznetsova A, Mawhinney DB, Naumenko V, Yates Jr JT, Li Q, Smalley RE. J Phys Chem B 2000;321:292.
[37] Chen S, Wu G, Liu Y, Long D. Macromolecules 2006;39:330.
[38] Wu HL, Yang YT, Ma CCM, Kuan HC. J Polym Sci Part A Polym Chem 2005;43:6084.
[39] Wu CS, Liao HT. J Polym Sci Part B Polym Phys 2003;41:351.
[40] Breitenbach A, Li YX, Kissel T. J Controlled Release 2000;64:167.
[41] Xu Y, Gao C, Kong H, Yan D, Jin YZ, Watts PCP. Macromolecules 2004;37:8846.
[42] Kashiwagi T, Grulke E, Hilding J, Harris R, Awad W, Douglas J. Macromolecular Rapid Commun 2002;23:761.
[43] Bom D, Andrews R, Sreekumar TV, Kumar S, Moore VC, Hauge RH, et al. Nano Lett 2002;2:615.
[44] Coleman JN, Cadek M, Blake R, Nicolosi V, Ryan KP, Belton C, et al. Adv Funct Mater 2004;14:791.
[45] Zhang X, Liu T, Sreekumar TV, Kumar S, Moore VC, Hauge RH, et al. Nano Lett 2003;3:1285.
[46] Liu L, Barber AH, Nuriel S, Wagner HD. Adv Funct Mater 2005; 15:975.
[47] Geng H, Rosen R, Zheng B, Shimoda H, Fleming L, Liu J, et al. Adv Mater 2002;14:1387.